OPEN ACCESS

University of BRISTOL

Kamsri, P., Punkvang, A., Hannongbua, S., Suttisintong, K., Kittakoop, P., Spencer, J., Mulholland, A. J., & Pungpo, P. (2019). In silico study directed towards identification of the key structural features of GyrB inhibitors targeting MTB DNA gyrase: HQSAR, CoMSIA and molecular dynamics simulations. *SAR and QSAR in Environmental Research*, *30*(11), 775-800. https://doi.org/10.1080/1062936X.2019.1658218

Peer reviewed version

Link to published version (if available):
10.1080/1062936X.2019.1658218

Link to publication record in Explore Bristol Research
PDF-document

This is the author accepted manuscript (AAM). The final published version (version of record) is available online via Taylor & Francis at https://www.tandfonline.com/doi/full/10.1080/1062936X.2019.1658218 . Please refer to any applicable terms of use of the publisher.

University of Bristol - Explore Bristol Research
General rights

This document is made available in accordance with publisher policies. Please cite only the published version using the reference above. Full terms of use are available:
http://www.bristol.ac.uk/red/research-policy/pure/user-guides/ebr-terms/

In silico Study Directed Towards Identification the Key Structural Feature of GyrB Inhibitors Targeting MTB DNA Gyrase: HQSAR, CoMSIA and Molecular Dynamics Simulations

Pharit Kamsri[a,*], Auradee Punkvang[a], Supa Hannongbua[b], Khomson Suttisintong[c], Prasat Kittakoop[d,e,f], James Spencer[g], Adrian J. Mulholland[h], and Pornpan Pungpo[i]

[a]*Division of Chemistry, Faculty of Science, Nakhon Phanom University, Nakhon Phanon, Thailand;* [b]*Department of Chemistry, Faculty of Science, Kasetsart University, Bangkok, Thailand;* [c]*National Nanotechnology Center, NSTDA, Pathum Thani, Thailand;* [d] *Chulabhorn Research Institute, Bangkok, Thailand;* [e] *Chulabhorn Graduate Institute, Chemical Biology Program, Chulabhorn Royal Academy, Bangkok, Thailand;* [f] *Center of Excellence on Environmental Health and Toxicology (EHT), CHE, Ministry of Education, Bangkok, Thailand ;* [g]*School of Cellular and Molecular Medicine, University of Bristol, Bristol, U.K.;* [h]*Centre for Computational Chemistry, School of Chemistry, University of Bristol, Bristol, U.K.;* [i]*Department of Chemistry, Faculty of Science, Ubon Ratchathani University, Ubon Ratchathani, Thailand*

***Corresponding authors**

[a]Pharit Kamsri

Division of Chemistry, Faculty of Science,

Nakhon Phanom University,

Nakhon Phanom, Thailand

E-mail: pharit.kamsri@npu.ac.th

Tel: +664 2503 776

In silico Study Directed Towards Identification the Key Structural Feature of GyrB Inhibitors Targeting MTB DNA Gyrase: HQSAR, CoMSIA and Molecular Dynamics Simulations

MTB DNA gyrase subunit B (GyrB) has been identified as promising target for rational drug design against fluoroquinolone drug resistant tuberculosis. In this study, we attempted to identify the key structural feature for highly potent GyrB inhibitors through 2D-QSAR using HQSAR, 3D-QSAR using CoMISA and MD simulations approaches on a series of thiazole urea core derivatives. The best HQSAR and CoMSIA models based on IC_{50} and MIC displayed the structural basis required for good activity against both GyrB enzyme and mycobacterial cell. MD simulations and binding free energy analysis using MM-GBSA and waterswap calculations revealed that urea core of inhibitors has strongest interaction with Asp79 via hydrogen bond interactions. In addition, cation-pi interaction and hydrophobic interactions of R_2 subsituent with Arg82 and Arg141 help to enhance the binding affinity in GyrB ATPase binding site. Thus, the present study beneficially provides crucial structural feature and a structural concept for rational design of novel DNA gyrase inhibitors with improved biological activities against both enzyme and mycobacterial cell; good pharmacokinetic properties and drug safely profiles.

Keywords: GyrB inhibitors; Binding free energy; CoMSIA; HQSAR; MD simulations, DNA gyrase

Introduction

Tuberculosis, TB caused by *Mycobacterium tuberculosis* (MTB) is one of the top 10 causes of death worldwide and the leading cause from a single infectious agent. There are 1.6 million deaths and 10.0 million people developed TB disease in 2017 [1]. Based on drug resistant tuberculosis, potential targets for tuberculosis drug development have been validated [2-4]. DNA gyrase had been identified as potential target for anti-tuberculosis drug discovery and the attractive target of fluoroquinolones, second-line drug for multidrug resistant tuberculosis (MDR-TB) [5-9]. This enzyme involved in the DNA replication mechanism. DNA gyrase consisted two subunits, DNA gyrase subunit A (GyrA) and DNA gyrase subunit B (GyrB) domains, in the holoenzyme complex as a heterotetramer A_2B_2 [10-12]. Only GyrA interacted with DNA and did the DNA cleavage

and relegation processes by tyrosine residue in the catalytic site [13,14], whereas the GyrB promoted the ATP hydrolysis to process the catalytic cycles [15]. Fluroquinolone drugs interacted with DNA in GyrA domain to create conformational changes of DNA gyrase enzyme [5]. However, resistance to fluoroquinolones may occur spontaneously due to the mutation of fluoroquinolone binding site leading to extensively drug resistant tuberculosis (XDR-TB) [16-19]. To overcome fluoroquinolone drug resistant, novel DNA gyrase inhibitors which shown the alternative inhibition mechanism at the ATPase binding site of GyrB were proposed [7-9] such as 4-aminoquinolines [20], thiazole–aminopiperidines [21], pyrrolamides [22], 2-amino-5-phenylthiophene-3-carboxamides [23], quinoline–aminopiperidines [24], benzofurans [25] and benzo[*d*]isothiazoles [26]. Thiazole urea cores derivatives [27, 28] were discovered as GyrB inhibitors by a scaffold-hopping approach. Some compounds showed good potency against GyrB enzyme and *M. tuberculosis* with high correlation between GyrB inhibitory activity and anti-microbial activity. Based on the promising results from this report, lead optimization process was required. However, these compounds show low pharmacokinetic properties. The optimization of thiazole urea derivatives to build good pharmacokinetic properties and safety profile were required. Recently, QSAR study have been applied to identify the structural requirement of DNA gyrase inhibitors including fluoroquinolone [29-31], isothiazoloquinolone [31] and quinoline-aminopiperidine [32] derivatives. However, information of the key structural features of inhibitors responsible to both enzyme and bacterial cell inhibition were not reported. In the present study, QSAR approaches and MD simulations were performed to gain insight into the key structural features of thiazole urea core derivatives responsible to GyrB and mycobacterial inhibitions. The obtained results revealed the key structural structure that serve as template in designing for high potency of DNA gyrase inhibitors. The finding concept in the present study were applied to design novel thiazole urea derivatives. In addition, pharmacokinetic properties of novel designed thiazole urea derivatives were considered. Compounds with high predictions of GyrB enzyme inhibition and mycobacterial inhibition that showed good pharmacokinetic properties were proposed.

Material and Methods

Compound dataset

55 thiazole urea core derivatives including thiazolopyridinone urea, thiazolopyridine urea and benzothiazole urea derivatives (Table 1) with GyrB ATPase inhibition activity (inhibition concentration of compound required for ATPase inhibition activity at 50% (IC_{50}) in nanomolar concentration unit) and anti-mycobacterial activity (minimum inhibitory concentration (MIC) in micromolar concentration unit) were collected from the literature [27, 28]. The general scaffolds, thiazolopyridinone urea (scaffold A), thiazolopyridine urea (scaffold B) and benzothiazole urea (scaffold C) of the molecules are depicted in Figure 1. These derivatives shared the thiazole urea core structure and the inhibitory activities against GyrB and mycobacterial cell of these inhibitors were measured by *M. smegmatis* GyrB ATPase assay and *M. tuberculosis* H37Rv cell on MABA assay in the same laboratory. The IC_{50} and MIC values of the collected thiazole urea derivatives are in the range from 0.5 to 217 nM and 0.06 to 21 µM. Three-dimensional coordinate of inhibitors was downloaded from CHEMBL database and used as initial coordinate for structure optimizations. M062X/6-31G* basis set implemented in Gaussian 09 program was applied for structural optimizations. The biological activities of thiazole urea core derivatives were converted into $\log(1/IC_{50})$ and log(1/MIC) for GyrB inhibitory activity and anti-mycobacterial activity to reduce the range of biological activities, which serves as dependent variable for QSAR study. Thiazole urea core derivatives were classified as two datasets, training set for QSAR model construction and test set for validations of QSAR model. 9 compounds of test set were selected by consideration of the structural diversity and the biological activity range of thiazole urea derivatives.

[Figure 1.]

[Table 1.]

HQSAR studies

HQSAR approach [32] was performed using SYBYL X-2.0 [33] to investigate the structural requirement for improving the biological activities. 55 GyrB inhibitors were

classified into two main classes, training set (46 compounds, 84 %) and test set (9 compounds, 16 %). For HQSAR analysis, four molecular fragments, atom (A), bond (B), component (C) and donor and acceptor (DA) were selected as the independent molecular descriptors and biological activities were used as dependent variable for HQSAR model contractions. To develop robust HQSAR models, numerous models with various combinations of the fragment-distinction properties were constructed. Partial least square (PLS) was used to contrast the models of relationship of HQSAR descriptors and biological activity ($\log(1/IC_{50})$ or $\log(1/MIC)$). The best HQSAR model was selected depending based on leave-one-out cross-validation (q^2) higher than 0.6, lower standard error (SE) value and the best cross-validated r^2.

3D-QSAR studies

CoMFA [34,35] and CoMSIA [36] approaches were performed using SYBYL X-2.0. The data set to set up CoMFA and CoMSIA model is the same set used in HQSAR approach. The pharmacophore alignment module with the Genetic Algorithm with Linear Assignment for Hypermolecular Alignment of Datasets (GALAHAD) was used as molecular alignment tool for thiazole urea derivatives. GALAHAD is a developed program that uses genetic algorithm (GA) to generate pharmacophore hypotheses by ranging of energy profile, specificity value, and Pareto ranking [37-40] based on shared pharmacophoric and pharmacosteric features. The best docking conformation of the most active compound, compound **51** was used as template coordinate for molecular alignment for 3D-QSAR CoMFA and CoMSIA studies. GALAHAD was run for 20 maximum iterations with a population size of 40 with 20 pharmacophore models creations. The conformation that aligned to best pharmacophore model was selected. CoMFA descriptors, steric (S) and electrostatic (E) were calculated in standard settings with the energy cut-off values of 30 kcal/mol. The CoMSIA similar indices descriptors including steric (S) and electrostatic (E), hydrophobic (H), hydrogen-bond donor (D) and hydrogen-bond acceptor (A) fields with attenuation factor α value of 0.3 and a grid spacing of 2 Å were calculated. After descriptor generation, PLS methodology was performed to find the correlation between dependent variables ($\log(1/IC_{50})$ or $\log(1/MIC)$) and independent variable (CoMFA and CoMSIA descriptors). The q^2 of model higher than 0.6 with highest r^2 were used to evaluate the predictive ability of 3D-QSAR models and used as the criteria to accept the best and reliable 3D-QSAR model.

Molecular docking calculations

GyrB ATPase domain of *Mycobacterium smegmatis* (*M. smegmatis*) complexed with RWX (2-[(3*S*,4*R*)-4-[(3-bromanyl-4-chloranyl-5-methyl-1*H*-pyrrol-2-yl)carbonyl amino] -3-methoxy-piperidin-1-yl]-4-(2-methyl-1,2,4-triazol-3-yl)-1,3-thiazole-5-carboxylic acid) (PDB code 4BAE) was downloaded from protein databank and was used as receptor coordinate for molecular docking [22]. Molecular docking was employed using Autodock 2.4 program. The docking parameter was validated by docking of RWX into the binding site. RWX ligand was used as centre of grid box (size 42×42×42 point) with 0.375 Å spacing. The defeat docking parameter with 300 run of Lamarckian Genetic Algorithm (LGA) were applied [41]. The RMSD between docked and x-ray conformation lower than 1 Å (0.72±0.06, n=3) was used as criteria for acceptable docking parameters. All selected thiazole urea core compounds for MD simulations were docked into the GyrB ATPase binding size using the same docking parameter of RWX compound. The lowest docking energy conformation was selected as the binding mode of thiazole urea cores in the active site of GyrB ATPase.

MD simulations

The binding mode and binding interactions of selected derivatives were discussed in the original paper of thiazole urea derivatives. However, these results were obtained from flexible-rigid docking calculations [28]. To obtain reliability and accuracy of the binding mode and binding interactions of thiazole derivative in GyrB ATPase binding site in the solvation system and full flexibility of GyrB ATPase, six thiazole urea core derivatives covering the range of the most active to low active compounds were selected for MD simulations. Compound **51** is represented as the most active compound with IC_{50} of 0.5 nM, whereas compounds **55** with IC_{50} value of 160 nM is representative compound possessing weak inhibitory activities against GyrB. Moreover, compounds **25**, **26**, **30** and **35** are represented as moderate compounds. The IC_{50} values of moderate compounds are in range of 3.7 to 88 nM. MD simulations using AMBER16 package [42] was employed to elucidate the binding model and their crucial binding interactions in GyrB ATPase domain. The initial structure of GyrB ATPase-thiazole urea core complexes were obtained from flexible-rigid docking calculations using Autodock 4.2 as described in molecular docking calculations section above. FF14SB [43] and general amber force field (GAFF) [44] were applied as parameter for GyrB ATPase and thiazole urea core ligands,

respectively. All missing hydrogen atoms of GyrB ATPase were added using the LEaP module. The restrained electrostatic potential (RESP) partial charges calculated at HF/6-31G* [45] were assigned as atomic charges of thiazole urea core ligands by the antechamber module implemented in the AMBER16 package. Each complex structure was solvated by cubic box of TIP3P [46] water molecules extending up to 10 Å from each solute species. Sodium cations (Na^+) were added to neutralize the charge of each system. To relax the bad steric interaction of water molecules and ions, the systems were first minimized with atomic positions of all solute species restraint (using a force constant of 500 kcal mol^{-1} $Å^{-2}$) with 2,500 steps of steepest descents followed by 20,000 steps of conjugated gradient. Non-bonded cut-off was set to 8 Å. Then, the system was gradually warmed up from 0 to 300 K in the first 20 ps followed by maintaining the temperature at 300 K in the last 10 ps with 2 fs time simulation steps with a restraint weight of 2 kcal mol^{-1} $Å^{-2}$. After minimization and heating step, the position-restrained dynamics simulations were applied to relax the positions of the solvent molecules for 70 ps at 300 K under an isobaric condition. Finally, 100 ns of MD simulations were performed for each system without any restraints. The long-range electrostatic interactions were treated by the Particle Mesh Ewald method (PME) [47] and the cut-off distance for the long-range van der Waals interaction was set to 8 Å. To constrain the bond lengths of hydrogen atoms attached to heteroatoms, the SHAKE method was applied [48].

Binding free energy calculations

Two binding free energy calculation approaches, MM-GBSA [49, 50] and waterswap calculations using Sire program [51, 52] were applied to estimate the binding affinity of GyrB ATPase-thiazole urea core inhibitor complexed. For MM-GBSA, 4,000 snapshots during last 40 ns of MD simulations (after reached the equilibrium state) were collected for the binding free energy calculations. Whereas, the waterswap calculation approach used the final coordinate (100 ns of simulations) as initial structure for binding free energy calculations.

Cluster analysis

Cluster analysis was performed to determine the structure populations from MD simulations, structure from last 40 ns of MD simulations were collected for clustering analysis using cpptraj module [53] with average linkage. Distance cut-off for forming

cluster was set at 1.5 Å. The average structure from the highest structure populations was selected for binding interaction analysis of thiazole urea cores in GyrB ATPase binding site.

Hydrogen bond analysis

The percentage and the number of hydrogen bond (H-bond) occupations between the selected thiazole urea core derivatives and the GyrB ATPase binding residues were identified according to the subsequent criteria: (i) the distance between hydrogen-bond donors (D) and hydrogen-bond acceptor (A) atoms ≤ 3.5 Å; and (ii) the D–H–A angle ≥150 by cpptraj module of AMBER16 to detect all hydrogen bonds during last 40 ns of MD simulations [53, 54].

Results and Discussion

QSAR models

The highest predictive ability for each developed HQSAR, CoMFA and CoMSIA models was shown in Table 2 and 3, respectively. The best HQSAR-IC_{50} model was obtained with q^2 and r^2 values of 0.62 and 0.91, respectively. For the best HQSAR-MIC model, q^2 and r^2 values were 0.60 and 0.90, respectively. The best model for HQSAR-IC_{50} and HQSAR-MIC contained three and four molecular fragment types which shared two combination fragment types, donor and acceptor features (DA) and connections (C). Only atoms (A) and bonds (B) were different combination to IC_{50} HQSAR and MIC HQSAR models, respectively. For 3D-QSAR model, only IC_{50} CoMSIA model including steric, electrostatic, hydrophobic and hydrogen donor fields was obtained with reliable q^2 value of 0.62 and r^2 of 0.98. The contribution of steric, electrostatic, hydrophobic and hydrogen donor fields is 15%, 33%, 27% and 25%, respectively, indicating that the electrostatic field shows greatest influence on the activity of thiazole derivatives against GyrB inhibitory activity. Predicted biological activity of training set of IC_{50} CoMSIA, IC_{50} HQSAR and MIC HQSAR models were predicted and summarized in Table 4. To access the predictive abilities of each models, IC_{50} and MIC values of the test set were predicted as concluded in Table 4. The predicted activities of the training set are close to the experimental activities with highest deviation values of 0.25, 0.43 and 0.69 logarithm unit for IC_{50} CoMSIA, IC_{50} HQSAR and MIC HQSAR models, respectively. In addition,

deviation values between experimental and predicted activity of test set for IC_{50} CoMSIA, IC_{50} HQSAR and MIC HQSAR models are 0.40, 0.40 and 0.44 (lower than one logarithm unit) indicated that the QSAR models obtained from this work can be utilized to predict the biological activity of newly design thiazole urea core derivatives. The experimental and predicted activities of the IC_{50} CoMSIA, IC_{50} HQSAR and MIC HQSAR models reveal a linear relationship (Figure 2).

[Table 2.]

[Table 3.]

[Table 4.]

[Figure 2.]

HQSAR atomic contribution and molecular fragment analysis

Molecular fragments of thiazole urea core derivatives which contribute directly to biological activities of GyrB inhibition (IC_{50}) and mycobacterial cell inhibition (MIC) can be visualized through HQSAR contribution maps. The HQSAR colour coding demonstrates the atomic contributions of the compounds with regards to biological activity. Green and yellow atomic contribution demonstrate a favourable contribution or positive contribution with regards to biological activity, whereas red, red-orange and orange indicate an unfavourable or negative contribution. White suggests an intermediate contribution of the atoms towards inhibitory activity. The atomic distributions of highest active compound **51**, moderate active compound **37** and low active compound **4** with IC_{50} HQSAR and MIC HQSAR were exposed in Figure 3. For the IC_{50} HQSAR model, the highest active compound **51** and moderate active compound **37** exhibited the important green and yellow fragments. In contrast, the lowest active compound (compound **4**) only showed the bad fragments, orange and red fragments. The colour code labelling of MIC HQSAR model reveals that thiazole urea core is crucial for inhibitory activity responsible for GyrB enzyme and mycobacterial cell. R_2 and R_3 are positively favourable for anti-mycobacterial activity as displayed in compound **51** (the highest active compound) and

compound **37** (moderate active compound). The low active compound **4** were labelled by orange and red colour labelling. These results demonstrated that thiazole urea cores is key fragment for favorable to high potency on IC_{50} and MIC. In addition, R_2 and R_3 substituents were favorable to improv the anti-mycobacterial activity.

[Figure 3.]

[Figure 4.]

CoMSIA contour maps

The structural requirement to improve GyrB inhibitory activity were derived from CoMSIA contour maps using the highest predictive ability IC_{50} CoMSIA model as displayed in Figure 5. The steric contour map was used to discriminate the steric structural requirement. Green and yellow contours were steric favourable and steric unfavourable, respectively. The electrostatic contour map was used to describe the effect of charge on the structural requirement of thizaole derivatives. Red and blue contour represent the negative charge and positive charge favourable, respectively. Magenta and white contour of CoMSIA hydrophobic contour map present the hydrophobic and hydrophilic properties favourable. The hydrogen bond donor and hydrogen bond favourable were suggested by cyan and purple contour maps, respectively. Cyan contour map located very closed to NH of urea fragment of thiazole urea core derivative indicate that hydrogen bond donor property of this fragment was required to enhance the biological activity. All data set compounds in this work contained this urea fragment. This is confirmed that urea part was crucial for biological activity of thiazole urea core derivatives. At R_1 position, there is only one small yellow contour appeared. Therefore, small substituent or low steric hindrance substituent was required to improve the GyrB inhibitory activity. For example, compound **21** and compound **22** contained allyl and ethyl substituent of thiazole urea core scaffold A, respectively. The inhibitory activity (IC_{50}) of compound **21** was 50 nM that showed the slightly higher inhibitory activity than compound **22** with IC_{50} value of 40 nM. Compound **27** and **28** that represented as member of thiazole urea core scaffold B were presented with allyl and ethyl substituents on R_1 position. Allyl substituent of compound **27** produced lower biological activity than ethyl substituent of compound **28** with the IC_{50} of 46 nM and 25 nM for compound **27** and **28**, respectively. At R_2 position, the green, red and white contours were displayed demonstrate that steric with negative

charge and hydrophilic properties were required for improving the biological activity of thiazole urea core derivatives. For the steric effect on R_2 substituent, compounds **7**, **9**, **11**, **14** and **15** showed difference biological activity against GyrB because of substituent size of R_2 position. The increasing size of 3-fluoro-pyrimidinyl (compound **7**), 3-methoxy-pyrimidinyl (compound **9**), 3-cyano-pyrimidinyl (compound **11**) and 1-alkyl-2(1*H*)-pyridinonyl (compound **14** and **15**)confirmed that the biological activity of thiazole urea core scaffold A (thiazolopyridinone) were increased for 10 nM, 6 nM, 4 nM, 5 nM and 2.5 nM for compounds **7**, **9**, **11**, **14** and **15**, respectively. The biological activity of compounds **44**, **45** and **46** (thiazole urea core scaffold B) demonstrate that increasing of substation on 3^{th} position of pyridininyl substituent R_2 enhanced the IC_{50} values of 12 nM, 10 nM and 4 nM for compounds **44**, **45** and **46**, respectively. In addition, increasing size of aromatic ring of R_2 substituent of thiazole urea core scaffold B were improved the biological activity as exemplified in compounds **46**, **47** and **51**. Compound **47** containing 1-methylpyrazole substituent at R_2 position showed the biological activity lower than compound **48** that contained 1-methyl-2(1*H*)-pyridinonyl substituent with IC_{50} values of 10 nM and 1 nM for compounds **47** and **48**, respectively. In addition, compound **51** containing larger substituent size on 2(1*H*)-pyridinonyl than compound **47** showed the potency higher with the value of 0.5 nM and 1 nM, respectively. As considered with the effect of electrostatic property on R_2 substituent, compounds **38**, **39**, **43**, **44** and **48** were exemplified. Replacing H atom on pyridinyl ring of R_2 substituent of compound **38** by high electronegativity fluorine atom (compound **39**) or CN group (compounds **43** and **44**) were considered. The biological activity of compounds **39** and **43** were increased as compared to compound **38** with the IC_{50} of 90 nM, 7 nM, 14 nM and 12 nM for compounds **38**, **39**, **43** and **44**, respectively. Adding an oxygen carbonyl on R_2 substituent, the biological activity of thiazole urea core derivative was increased as depicted by compounds **38** and **48**. Pyridinyl substituent on compound **38** produced low biological activity than 1-methyl-2(1*H*)-pyridinonyl substituent on compound **48**. The effect of hydrophobic property and hydrophilic properties of R_2 position on the biological activity of thiazole urea core derivative was discriminated by compounds **6** and **18** in scaffold A. Compound **6** showed the inhibitory activity higher than **18** due to more hydrophilic favourable of pyrimidine of compound **6** as compared to pyridine ring of compound **18**. Compounds **48**-**50** were used to exemplify the effect of hydrophilic property of R_2 position on thiazole urea core scaffold B derivatives. The increasing hydrophobic property of compounds **49** and **50** effected to lower inhibitory activity than compound **48**.

At R_3 position of scaffold B, this position required the steric substituent to improve the biological activity. For example, compound **27** showed high potency than compound **26** due to the steric substituent. In addition, compound **30** contained heterocyclic aliphatic substituent which they showed the potency higher than compound **34** (linear aliphatic chain). The hydrophobic substituent improved the biological activity of thiazole urea core scaffold B. For example, compounds **30**, **31** and **32** which contained different R_3 substituent showed different inhibitory activities. Compound **30** with 3-methyltetrahydrofuran displayed the potency higher than compounds **31** and **32** that contained tetrahydropyran and tetrahydrofuran substituents, respectively.

[Figure 5.]

MD simulations

The root-mean square deviations (RMSD) over the simulations time of solute species, GyrB ATPase and selected ligands were calculated and plotted as shown in Figure 6. MD simulations systems of GyrB ATPase and selected ligands reach the equilibrium state after 40 ns, 50 ns, 30 ns, 60 ns, 10 ns and 10 ns for compounds **25**, **26**, **30**, **35**, **51** and **55**, respectively. Therefore, the MD snapshots after 60 ns of the simulations time were selected for binding free energy calculations and structural analysis.

[Figure 6.]

The binding free energy of thiazole urea cores complexed with GyrB ATPase with two calculation methods were summarised in Table 4 and Figure 7. Both binding free calculation methods were corrected order of active compounds. The correlation (R^2) between experimental binding free energy and calculated binding free energy from MM-GBSA and waterswap are 0.52 and 0.85, respectively. In addition, waterswap calculations showed higher correlation than MM-GBSA approach. These results indicated that the binding mode of thiazole urea core derivatives are corrected based on the correlation between experimental and calculated binding free energy approved. The obtained results

from these binding energy calculations demonstrated that the conformation obtained from MD simulations can produced the corrected order of binding free energy and GyrB inhibitory activity. Therefore, the finding binding mode from MD simulations is reliable for investigation of the binding mode and crucial interactions for binding of thiazole urea core derivatives in the GyrB ATPase domain.

[Table 4.]

[Figure 7.]

The binding interactions of thiazole urea core derivatives in GyrB ATPase domain

The binding mode of thiazole urea core derivatives was examined to investigate the key binding interactions in GyrB ATPase binding site. The binding interactions of the highest active compound **51** was analysed and showed in Figure 8. Compound **51** formed two hydrogen bond interactions with Asp79 and Arg141. A NH of urea fragment of thiazole urea core compound **51** interacted with oxygen atoms of Asp79 sidechain. Hydrogen atom of Asn52 point to thiazole aromatic ring of inhibitor and formed sigma-pi interaction. Glu56 sidechain closed to thiazole ring and formed van der Waals interaction. Ethyl R_1 substituent interacted with hydrophobic interaction with Val49, Ala53, Val65, Val77, Thr169 and Ile171 sidechain. An oxygen carbonyl of R_2 substituent from hydrogen bond interaction with NH sidechain of Arg141. Cation-pi was obtained between guanidinium cation sidechain of Arg82 with aromatic ring of R_2 substituent of compound **51**. In addition, hydrophobic interactions of R_2 substituent of this compound 51 with Arg82, Gly83 and Pro85 were achieved. For R_3 substituent of compound **51**, this substituent contacted with Ile84, Pro85, Thr95, Val99, Leu120 and Val123 sidechains by hydrophobic interactions. These results were supported by the interaction energy using MM-GBSA calculation and hydrogen bond analysis as shown in Figure 9 and Figure 10. Figure 9e showed the binding interactions energy of compound **51**. Large energy contribution was observed from the interaction of compound **51** with Asp79 with -12.0 kcal/mol. In addition, the interaction energy of Arg141 with an oxygen of carbonyl group support the strong binding affinity of compound **51** with -8.1 kcal/mol. For all selected

compounds, the binding interaction energy profiles were similar to the energy profile of compound **51** due to hydrogen bon interaction of nitrogen atom on pyridinyl substituent with Arg141, except compound **25**. Compound **25** formed additional hydrogen bond interaction between an oxygen carbonyl of urea core with NH sidechain of Asn52. Based on six selected compounds for MD simulation in this study, we found that three residues, Asn52, Asp79 and Arg141 of GyrB ATPase formed hydrogen interaction with thiazole urea core derivatives as shown in Figure 10. An oxygen atom of Asp79 sidechain act as hydrogen bond acceptor to bind with NH of urea of thiazole urea core derivatives along the hydrogen bond interaction with % hydrogen bond occupation higher than 50 %. This result suggested that hydrogen bond interactions were crucial interaction for binding with GyrB ATPase domain of thiazole urea core derivative via the hydrogen bond interactions with Asp79. In addition, hydrogen bond interaction with Arg141 of R_2 substituents improved the biological activity of thiazole urea core derivatives against GyrB as shown in Figure 10. As compared to the docking results from original paper, the crucial interactions in ATPase binding site were similar. Asp79 interacted with NH of urea core via hydrogen bond interactions. Hydrogen bond interactions of an oxygen carbonyl and NH of Arg141 sidechain was also reported [28]. However, there are no hydrogen bond linker interactions water molecules by of nitrogen atom of thiazole ring with oxygen carbonyl of Asp79 sidechain and an oxygen carbonyl of urea core with NH of Asn52 based on MD simulations and waterswap calculations in the present study. Therefore, water molecule doesn't affect to the binding interactions of thiazole urea derivatives in ATPase binding site.

[Figure 8.]

[Figure 9.]

[Figure 10.]

The key structural feature of thiazole derivatives for highly potent biological activities

In the present study, well-known QSAR approaches were carried out to understand the key structural requirements of thiazole urea derivatives responsible to both GyrB enzyme and mycobacterial cell. These finding provides the critical information to rational design of new highly potent thiazole urea inhibitors. Based on the MD simulations results, the quantitative information of binding mode and binding interactions

was obtained from the solvation system by high accuracy of calculation method. The integrations of QSAR and MD simulations results provided the essential structural features for rational design of new and highly potent inhibitors with specific to GyrB ATPase binding site. The structural requirements and key interaction for binding of thiazole urea core derivatives for good potency against both IC_{50} and MIC derived from QSAR models and MD simulations approaches were summarized in Figure 11. Based on HQSAR, CoMSIA and MD simulations, the common structural features required for inhibition of GyrB enzyme and mycobacterial cell are revealed. The results of HQSAR based on two different biological activities, IC_{50} and MIC, suggest that the thiazole urea core was the key structure to obtain the inhibitory activities against both GyrB enzyme and mycobacterial cell. Urea fragment structure of thiazole urea core derivatives was crucial fragment for binding in GyrB ATPase binding pocket with hydrogen bond interactions with Asp79. These results demonstrated that thiazole urea core should be kept for good potency against both enzyme and bacterial cell. To improve the potencies, small substituent at R_1 position was required to interact with hydrophobic side chain of GyrB. A R_2 position, steric substituent like heterocyclic aromatic ring with hydrophilic property and suitable position of negative charge were required to bind with Arg82, Arg141 and hydrophobic residues via hydrogen bond interaction, cation-pi interaction and hydrophobic interactions, respectively. For R_3 position, steric substituent with hydrophobic property was required to enhance the inhibitory activities of thiazole urea core derivatives. An extensive analysis of QSAR and MD simulations was very useful to design new drug candidates against GyrB ATPase targets. In addition, QSAR models can be an useful tool to guide further inhibitors design studies for the optimizations and development of new thiazole ureas having improved GyrB ATPase binding affinity. Considering the results obtained in the present study, the improvement of lead and candidate of the DNA gyrase inhibitors status in a series of thiazole urea derivatives.

[Figure 11.]

Rational design of novel thiazole urea derivatives

Novel thiazole urea derivatives were designed based on our obtained results. The R_2 and R_3 substituents were modified, whereas thiazole urea core and the ethyl R_1 substituent were kept as the general structure. Heterocyclic aromatic rings were added to

the R_2 position with the aim for forming the cation-pi interaction with Arg82. Steric substituents with hydrophobic property were introduced to the R_3 position. For designing new DNA gyrase inhibitors, the physicochemical properties and pan assay interference compounds (PAINS) violation were considered for the novel DNA gyrase inhibitors using SwissADME prediction [55]. The HQSAR-IC_{50} and HQSAR-MIC models were used to predict the biological activities of novel thiazole urea derivatives. 1,200 novel thiazole urea derivatives were designed based on the finding key structural features. In general, the log(1/IC_{50}) and log(1/MIC) higher than 7.00 and 6.00 were required as potent GyrB inhibitor of thiazole urea derivative [28]. Based on HQSAR-IC_{50} and HQSAR-MIC predictions, 407 thiazole urea derivatives were collected based on log(1/IC_{50}) and log(1/MIC) prediction higher than 7.00 and 6.00, respectively. preADME [56] was applied to predict the pharmacokinetic parameters of novel designed compounds as well as the most active compound **51** as shown in Table 5. The most active compound **51** displayed low blood-brain barrier (BBB) penetration and plasma protein binding (PPB) with the values of 0.02 and 49.66%, respectively. Moderate value of MadinDarby Canine Kidney (MDCK) cell models for oral drug absorption was obtained with the value of 4.64. High heterogeneous human epithelial colorectal adenocarcinoma cell lines (Caco2-cell) and HIA were obtained with the values of 38.87 and 94.70, respectively. The BBB values of designed thiazole urea derivatives higher than the most active compound **51** (>0.02) were considered. 200 compounds (Table S1) display the BBB values higher than the most active compound **51**. **D007** and **D063** showed the highest predicted log(1/IC_{50}) and log(1/MIC) with the values of 8.40 and 6.51, respectively. Their structures drug like properties and pharmacokinetic were summarized in Figure 12 and Table 5. The pharmacokinetic properties of designed compounds were acceptable, except MDCK cell level. Interestingly, PPB of novel designed compounds were higher than the most active compound **51**. The binding modes of **D007** and **D063** were predicted using docking calculations. The binding energies of compounds **D007** and **D063** are -9.66 and -7.97 kcal/mol, respectivelyindicating that these compounds are favourable for binding in ATPase domain of GyrB. The predicted binding modes of compounds **D007** and **D063** in ATPase binding pocket are shown in Figures 13a and 13b, respectively. NH of the urea core structure interacts with the oxygen carboxylate of Asp79 sidechain by hydrogen bond interactions. Cation-pi interaction with Arg82 was found between the aromatic R_2 substituent of both compounds (**D007** and **D063**). In addition, the nitrogen atoms on pyrimidine ring of **D007** and oxadiazole ring of **D063** form the hydrogen bond

interactions with Arg141. These results demonstrated that the novel designed compounds can be proposed as new DNA gyrase inhibitors with good pharmacokinetic properties and strongly bind with ATPase domain.

[Figure 12]

[Table 5]

[Figure 13]

Conclusion

The key structural features of thiazole urea core derivative responsible for high potency against of GyrB and mycobacterial cell inhibition were successfully investigated by HQSAR, CoMSIA and MD simulations. IC_{50} HQSAR, MIC HQSAR and IC_{50} CoMSIA models have high power to predict the activities of thiazole urea core derivatives. The reliable binding modes, binding free energy, and binding interactions of thiazole urea core derivatives in the GyrB ATPase binding pocket were obtained by MD simulations. Based on MD simulations, the crucial interactions of thiazole urea derivatives were corresponded well to previously report from the original paper. In contrast, water molecules were not stabilized the hydrogen interactions of thiazole urea derivatives with amino acid residues surrounding their binding site. The combination of graphical interpretation of QSAR results and MD simulations provides a key insight into the structural features needed to increase the IC_{50} and MIC values of thiazole urea core derivatives. Thiazole urea core and R_2 substituent were required to attaining favorable IC_{50} and MIC values, whereas the R_3 substituent is the key to enhance the potency against IC_{50}. Therefore, the results obtained from this study should facilitate the further modification of thiazole urea core derivatives for generating novel DNA gyrase inhibitors with improved GyrB and mycobacterial cell inhibition potency. Therefore, novel thiazole urea derivatives with good predicted biological activities and pharmacokinetic properties were proposed as potent DNA gyrase inhibitors.

Acknowledgements

This research was supported by the Thailand Research Fund (MRG6180147 and RSA5980057) and the Health Systems Research Institute (HSRI.60.083). This work has been facilitated by the BrisSynBio Biosuite (UK Biotechnology and Biological Sciences

(BBSRC) and Engineering and Physical Sciences (EPSRC) Research Councils, BB/L01386X/1) and the BBSRC ALERT14 equipment initiative (BB/M012107/1). AJM and JS acknowledge funding from the BristolBridge antimicrobial resistance network (EPSRC EP/M027546/1). We thank CCP-BioSim (grant number EP/M022609/1) for funding. The University of Bristol are gratefully acknowledged for computational resource supports of this research. Nakhon Phanom University, Ubon Ratchathani University, NECTEC and University of Bristol are gratefully acknowledged for supporting this research.

References

[1] https://www.who.int/tb/publications/global_report/GraphicExecutiveSummary.pdf?ua=1

[2] R. Dhiman and R. Singh, *Recent advances for identification of new scaffolds and drug targets for Mycobacterium tuberculosis*, IUBMB Life. 70(9) (2004), pp. 905-916.

[3] A. Bahuguna and D.S. Rawat, *An overview of new antitubercular drugs, drug candidates, and their targets*, Med. Res. Rev. (2019), https://doi.org/10.1002/med.21602.

[4] A.K. Saxena and A. Singh, *Mycobacterial tuberculosis Enzyme Targets and their Inhibitors*, Curr Top Med Chem. 19 (2019), pp. 337-355.

[5] J.M., Blondeau, *Fluoroquinolones: Mechanism of action, classification, and development of resistance*, Surv. Ophthalmol. 49 (2004), pp. S73-78.

[6] K. Mdluli and Z. Ma, *Mycobacterium tuberculosis DNA gyrase as a target for drug discovery*, Infect. Disord. Drug. Targets. 7 (2007), pp. 159-168.

[7] A. Kashyap, P.K. Singh and O. Silakari, *Chemical classes targeting energy supplying GyrB domain of Mycobacterium tuberculosis*, Tuberculosis (Edinb). 113 (2018), pp. 43-54.

[8] K. Chaudhari, S. Surana, P. Jain and H.M. Patel, *Mycobacterium tuberculosis (MTB) GyrB inhibitors: An attractive approach for developing novel drugs against TB*. Eur. J. Med. Chem. 124 (2016), pp. 160-185.

[9] V. Nagaraja, A.A. Godbole, S.R. Henderson and A. Maxwell, *DNA topoisomerase I and DNA gyrase as targets for TB therapy*, Drug Discov. Today. 22 (2017), pp. 510-518.

[10] K.J. Aldred, R.J. Kerns and N. Osheroff, *Mechanism of quinolone action and resistance*, Biochemistry. 53 (2014), pp. 1565-1574.

[11] T. Khan, K. Sankhe, V. Suvarna, A. Sherje, K. Patel and B. Dravyakar, *DNA gyrase inhibitors: Progress and synthesis of potent compounds as antibacterial agents*, Biomed. Pharmacother. 103 (2018), pp. 923-938.

[12] J.H. Morais Cabral, A.P. Jackson, C.V. Smith, N. Shikotra, A. Maxwell and R.C. Liddington, *Crystal structure of the breakage-reunion domain of DNA gyrase*, Nature. 388 (1997), pp. 903-906.

[13] B.D. Bax, P.F. Chan, D.S. Eggleston, A. Fosberry, D.R. Gentry, F. Gorrec, I. Giordano, M.M. Hann, A. Hennessy, M. Hibbs, J. Huang, E. Jones, J. Jones, K.K. Brown, C.J. Lewis, E.W. May, M.R. Saunders, O. Singh, C.E. Spitzfaden, C. Shen, A. Shillings, A.J. Theobald, A. Wohlkonig, N.D. Pearson and M.N. Gwynn, Type IIA topoisomerase inhibition by a new class of antibacterial agents, *Type IIA topoisomerase inhibition by a new class of antibacterial agents*, Nature. 466 (2010), pp.935-940.

[14] F. Collin, S. Karkare and A. Maxwell, *Exploiting bacterial DNA gyrase as a drug target: current state and perspectives*, Appl. Microbiol. Biotechnol. 92 (2011), pp. 479-497.

[15] A. Agrawal, M. Roué, C. Spitzfaden, S. Petrella, A. Aubry, M. Hann, B. Bax and C. Mayer, *Mycobacterium tuberculosis DNA gyrase ATPase domain structures suggest a dissociative mechanism that explains how ATP hydrolysis is coupled to domain motion*, Biochem. J. 456 (2013), pp. 263-273.

[16] E. Avalos, D. Catanzaro, A. Catanzaro, T. Ganiats, S. Brodine, J. Alcaraz and T. Rodwell, *Frequency and geographic distribution of gyrA and gyrB mutations associated with fluoroquinolone resistance in clinical Mycobacterium tuberculosis isolates: a systematic review*, PLoS One. 10 (2015), pp. e0120470.

[17] A. Von Groll, A. Martin, P. Jureen, S. Hoffner, P. Vandamme, F. Portaels, P.C. Palomino and P.A. da Silva, *Fluoroquinolone resistance in Mycobacterium tuberculosis and mutations in gyrA and gyrB*, Antimicrob. Agents Chemother. 53 (2009), pp. 4498-4500.

[18] A.S. Ginsburg, J.H. Grosset and W.R. Bishai, *Fluoroquinolones, tuberculosis, and resistance*, Lancet Infect. Dis. 3 (2003), pp. 432-442.

[19] F. Maruri, T.R. Sterling, A.W. Kaiga, A. Blackman, Y.F. van der Heijden, C. Mayer, E. Cambau and A. Aubry, *A systematic review of gyrase mutations associated with fluoroquinolone-resistant Mycobacterium tuberculosis and a proposed gyrase numbering system, J. Antimicrob*. Chemother. 67 (2012), pp. 819-831.

[20] B. Medapi, P. Suryadevara, J. Renuka, J.P. Sridevi, P. Yogeeswari and D. Sriram, *4-Aminoquinoline derivatives as novel Mycobacterium tuberculosis GyrB inhibitors: Structural optimization, synthesis and biological evaluation*, Eur. J. Med. Chem. 103 (2015), pp. 1-16.

[21] V.U. Jeankumar, J. Renuka, P. Santosh, V. Soni, J.P. Sridevi, P. Suryadevara, P. Yogeeswari and D. Sriram, *Thiazole-aminopiperidine hybrid analogues: design and synthesis of novel Mycobacterium tuberculosis GyrB inhibitors*, Eur. J. Med. Chem. 70 (2013), pp. 143-153.

[22] S.H. P, S. Solapure, K. Mukherjee, V. Nandi, D. Waterson, R. Shandil, M. Balganesh, V.K. Sambandamurthy, A.K. Raichurkar, A. Deshpande, A. Ghosh, D. Awasthy, G. Shanbhag, G. Sheikh, H. McMiken, J. Puttur, J. Reddy, J. Werngren, J. Read, R.M. Kumar M, M. Chinnapattu, P. Madhavapeddi, P. Manjrekar, R. Basu, S. Gaonka, S. Sharma, S. Hoffner, V. Humnabadkar, V. Subbulakshmi and V. Panduga, *Optimization of pyrrolamides as mycobacterial GyrB ATPase inhibitors: structure-activity relationship and in vivo efficacy in a mouse model of tuberculosis*, Antimicrob. Agents Chemother. 58 (2014), pp. 61-70.

[23] S. Saxena, G. Samala, J. Renuka, Y.P. Sridevi, P. Yogeeswari and D. Sriram, *Development of 2-amino-5-phenylthiophene-3-carboxamide derivatives as novel inhibitors of Mycobacterium tuberculosis DNA GyrB domain*, Bioorg. Med. Chem. 23 (2015), pp. 1402-1412.

[24] B. Medapi, J. Renuka, S. Saxena, J.P. Sridevi, R. Medishetti, P. Kulkarni, P. Yogeeswari and D. Sriram, *Design and synthesis of novel quinoline-aminopiperidine hybrid analogues as Mycobacterium tuberculosis DNA gyraseB inhibitors*, Bioorg. Med. Chem. 23 (2015), pp. 2062-2078.

[25] J. Renuka, K.I. Reddy, K. Srihari, V.U. Jeankumar, M. Shravan, J.P. Sridevi, P. Yogeeswari, K.S. Babu and D. Sriram D, *Design, synthesis, biological evaluation of substituted benzofurans as DNA gyraseB inhibitors of Mycobacterium tuberculosis*, Bioorg. Med. Chem. 22 (2014), pp. 4924-4934.

[26] K.I. Reddy, K. Srihari, J. Renuka, K.S. Sree, A. Chuppala, V.U. Jeankumar, J.P. Sridevi, K.S. Babu, P. Yogeeswari and D. Sriram, *An efficient synthesis and biological screening of benzofuran and benzo[d]isothiazole derivatives for Mycobacterium tuberculosis DNA GyrB inhibition*, Bioorg. Med. Chem. 22 (2014), pp. 6552-6563.

[27] R.R. Kale, M.G. Kale, D. Waterson, A. Raichurkar, S.P. Hameed, M.R. Manjunatha, B.K. Kishore Reddy, K. Malolanarasimhan, V. Shinde, K. Koushik, L.K. Jena, S. Menasinakai, V. Humnabadkar, P. Madhavapeddi, H. Basavarajappa, S. Sharma, R. Nandishaiah, K.N. Mahesh Kumar, S. Ganguly, V. Ahuja, S. Gaonkar, C.N. Naveen Kumar, D. Ogg D, P.A. Boriack-Sjodin, V.K. Sambandamurthy, S.M. de Sousa and S.R. Ghorpade, *Thiazolopyridone ureas as DNA gyrase B inhibitors: Optimization of antitubercular activity and efficacy*, Bioorg. Med. Chem. Lett. 24 (2014), pp. 870-879.

[28] M.G. Kale, A. Raichurkar, S.H. P, D. Waterson, D. McKinney, M.R. Manjunatha, U. Kranthi, K. Koushik, Lk. Jena, V. Shinde, S. Rudrapatna, S. Barde, V. Humnabadkar, P. Madhavapeddi, H. Basavarajappa, A. Ghosh, V.K. Ramya, S. Guptha, S. Sharma, P. Vachaspati, K.N. Kumar, J. Giridhar, J. Reddy, V. Panduga, S. Ganguly, V. Ahuja, S. Gaonkar, C.N. Kumar, D. Ogg, J.A. Tucker, P.A. Boriack-Sjodin, S.M. de Sousa, V.K. Sambandamurthy and S.R. Ghorpade, *Thiazolopyridine ureas as novel antitubercular agents acting through inhibition of DNA gyrase B*, J. Med. Chem. 56 (2013), pp. 8834-8848.

[29] Dipiksh, M. Salman and S. Nandi, *QSAR and pharmacophore modeling of anti-tubercular 6-Fluoroquinolone compounds utilizing calculated structural descriptors*, Med. Chem. Res. 26 (2017), pp. 1903-1914.

[30] N. Minovski, M. Vracko and T. Šolmajer, *Quantitative structure–activity relationship study of antitubercular fluoroquinolones*, Mol. Divers.15 (2011), pp. 417-426.

[31] S. Nandi, S. Ahmed and A.K. Saxena, *Combinatorial design and virtual screening of potent anti-tubercular fluoroquinolone and isothiazoloquinolone compounds utilizing QSAR and pharmacophore modelling*, SAR QSAR Environ. Res. 29 (2018), pp. 151-170.

[32] TRIPOS Associates, Inc, Sybyl-X Molecular Modeling Software Packages, St. Louis, MO, 498 USA, 2012.

[33] SYBYL-X 2.0. Tripos Inc., St. Louis, MO, 2015.

[34] R.D. Cramer, D.E. Patterson and J.D. Bunce, *Comparative molecular field analysis (CoMFA). 1. Effect of shape on binding of steroids to carrier proteins*, J. Am. Chem. Soc. 110 (1988), pp. 5959-5967.

[35] M. Clark, R.D. Cramer III, D.M. Jones, D.E. Patterson and P.E. Simeroth, Comparative molecular field analysis (CoMFA). 2. Toward its use with 3D-structural databases, Tetrahedron Comput. Methodol. 3 (1990), pp. 47-59.

[36] G. Klebe, U. Abraham and T. Mietzner, *Molecular similarity indices in a comparative analysis (CoMSIA) of drug molecules to correlate and predict their biological activity*, J. Med. Chem. 37 (1994), pp. 4130-4146.

[37] N.J. Richmond., CA. Abrams, P.R. Wolohan, E. Abrahamian, P. Willett and R.D. Clark, *GALAHAD: 1. pharmacophore identification by hypermolecular alignment of ligands in 3D*, J. Comput. Aided. Mol. Des. 20 (2006), pp. 567-587.

[38] Y. Xiang, Z. Hou and Z. Zhang, *Pharmacophore and QSAR studies to design novel histone deacetylase 2 inhibitors*, Chem. Biol. Drug Des. 79 (2012), pp. 760–770.

[39] R. Uddin, M. U. Lodhi and Z. Ul-Haq, *Combined pharmacophore and 3D-QSAR study on a series of Staphylococcus aureus Sortase A inhibitors*, Chem. Biol. Drug Des. 80 (2012), pp. 300–314.

[40] K.C. Weber, L.B. Salum, K.M. Honório, A.D. Andricopulo and A.B. da Silva, *Pharmacophore-based 3D QSAR studies on a series of high affinity 5-HT$_{1A}$ receptor ligands*, Eur. J. Med. Chem. 45 (2010), pp. 1508-1514.

[41] R. Huey, G.M. Morris, A.J. Olson and D.S. Goodsell, A semiempirical free energy force field with charge-based desolvation, J. Comput. Chem. 28 (2007), pp. 1145-1152.

[42] P.A.K. D.A. Case, R.M. Betz, W. Botello-Smith, D.S. Cerutti, T.E. Cheatham III, T.A. Darden, R.E. Duke, T.J. Giese, H. Gohlke, A.W. Goetz, N. Homeyer, S. Izadi, P.

Janowski, J. Kaus, A. Kovalenko, T.S. Lee, S. LeGrand, P. Li, C. Lin, T. Luchko, R. Luo, B. Madej, AMBER 2016, Univ. Calif. San Fr.

[43] C. Simmerling, *ff 14SB: Improving the accuracy of protein side chain and backbone parameters from ff 99SB*, J. Chem. Theory Comput. 11 (2015), pp. 3696–3713.

[44] J. Wang, R.M. Wolf, J.W. Caldwell, P.A. Kollman, and D.A. Case, *Development and testing of a general amber force field*, J. Comput. Chem. 25 (2004), pp. 1157–1174.

[45] W.D. Cornell, P. Cieplak, C.I. Bayly and P.A. Kollman, *Application of RESP charges to calculate conformational energies, hydrogen bond energies, and free energies of solvation*, J. Am. Chem. Soc.115 (1993), pp. 9620-9631.

[46] M.W. Mahoney and W.L. Jorgensen, *A five-site model for liquid water and the reproduction of the density anomaly by rigid, nonpolarizable potential functions*, J. Chem. Phys. 112 (2000), pp. 8910-8922.

[47] T. Darden, D. York and L. Pedersen, *Particle mesh Ewald: An N·log(N) method for Ewald sums in large systems*, J. Chem. Phys. 98 (1993), pp. 10089-10092.

[48] J.P. Ryckaert, G. Ciccotti and H.J.C. Berendsen, *Numerical integration of the cartesian equations of motion of a system with constraints: molecular dynamics of n-alkanes*, J. Comput. Phys., 23 (1977), pp. 327–341.

[49] B.R. Miller, T.D. Mcgee, J.M. Swails, N. Homeyer, H. Gohlke, and A.E. Roitberg, *MPBSA.py: An efficient program for end-state free energy calculations*, J. Chem. Theory Comput. 8 (2012), pp. 3314–3321.

[50] S. Genheden and U. Ryde, *The MM/PBSA and MM/GBSA methods to estimate ligand-binding affinities*, Expert Opin. Drug Discov. 10 (2015), pp. 449–461.

[51] C.J. Woods, M. Malaisree, S. Hannongbua, A.J. Mulholland, *A water-swap reaction coordinate for the calculation of absolute protein–ligand binding free energies*, J. Chem. Phys. 134 (2011), pp. 054114.

[52] C.J. Woods, M. Malaisree, J. Michel, B. Long, S. McIntosh-Smith and A.J. Mulholland, *Rapid decomposition and visualisation of protein–ligand binding free energies by residue and by water*, Faraday Discuss. 169(2014), pp. 477-499.

[53] D.R. Roe and T.E. 3rd Cheatham, *PTRAJ and CPPTRAJ: Software for processing and analysis of molecular dynamics trajectory data*, J. Chem. Theory. Comput. 9 (2013), pp. 3084-3095.

[54] K. Wendler, J. Thar, S. Zahn and B. Kirchner, *Estimating the hydrogen bond energy*, J. Phys. Chem. A. 144 (2010), 9529-9536.

[55] A. Daina, O. Michielin and V. Zoete, *SwissADME: a free web tool to evaluate pharmacokinetics, drug-likeness and medicinal chemistry friendliness of small molecules*, Sci. Rep. 7 (2017), pp. 42717.

[56] S.K. Lee, I.H. Lee, H.J. Kim, G.S. Chang, J.E. Chung and K.T. No, The PreADME approach: web-based program for rapid prediction of physico-chemical, drug absorption and drug-like properties, EuroQSAR 2002 designing drugs and crop protectants: processes, problems and solutions. Blackwell Publishing, MA, (2003) pp 418–420.

Table captions

Table 1. Structure and biological activities of thiazole urea core derivatives.

Cpd.	Scaffold	R_1	R_3	R_2	IC_{50} (nM)	MIC (μM)	$\log(1/IC_{50})$	$\log(1/MIC)$
1	A	Ethyl	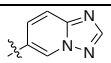	Isopropyl	11	1.3	7.96	5.89
2*	A	Ethyl	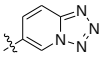	Isopropyl	20	3	7.70	5.52
3	A	Ethyl	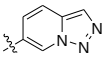	Isopropyl	16	0.8	7.80	6.10
4	A	Ethyl	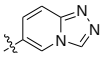	Isopropyl	217	12.5	6.66	4.90
5*	A	Ethyl	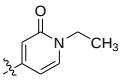	Isopropyl	2.5	0.2	8.60	6.70
6	A	Ethyl		Isopropyl	23	2	7.64	5.70
7	A	Ethyl		Isopropyl	10	11	8.00	4.96
8	A	Ethyl	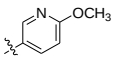	Isopropyl	23	10	7.64	5.00
9	A	Ethyl	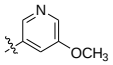	Isopropyl	6	4	8.22	5.40
10	A	Ethyl		Isopropyl	15	21	7.82	4.68
11	A	Ethyl		Isopropyl	4	4	8.40	5.40
12	A	Ethyl	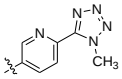	Isopropyl	20	1.6	7.70	5.80
13	A	Ethyl	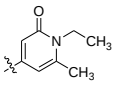	Isopropyl	5	0.5	8.30	6.30
14*	A	Ethyl	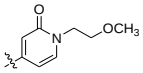	Isopropyl	5	0.3	8.30	6.52
15	A	Ethyl	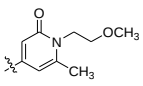	Isopropyl	2.5	0.3	8.60	6.52
16	A	Ethyl		H	84	9	7.08	5.05
17	A	Ethyl		Ethyl	30	2	7.52	5.70

18	A	Ethyl		Isopropyl	40	2	7.40	5.70
19	A	Ethyl			40	3	7.40	5.52
20*	A	Ethyl			25	8	7.60	5.10
21	A	Allyl		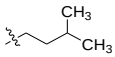	50	10	7.30	5.00
22	A	Ethyl		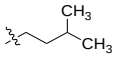	40	7.3	7.40	5.14
23	A	Ethyl			14	3	7.85	5.52
24	B	Ethyl		Methoxy	22	2	7.66	5.70
25	B	Ethyl	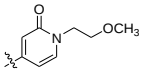		3.7	0.27	8.43	6.57
26	B	Allyl		H	88	8	7.06	5.10
27	B	Allyl		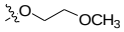	46	10	7.34	5.00
28	B	Ethyl		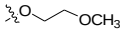	25	2.8	7.60	5.55
29	B	Ethyl		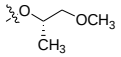	12	1.29	7.92	5.89
30	B	Ethyl		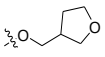	5	1.3	8.30	5.89
31	B	Ethyl			9	0.92	8.05	6.04
32*	B	Ethyl			13	1.54	7.89	5.81
33	B	Ethyl			39	0.92	7.41	6.04
34	B	Ethyl		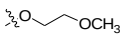	17	0.67	7.77	6.17
35	B	Ethyl		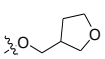	10	0.2	8.00	6.70
36*	B	Ethyl			30	2	7.52	5.70
37	B	Ethyl			30	1	7.52	6.00
38	B	Ethyl			90	3.5	7.05	5.46

39	B	Ethyl		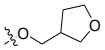	7	0.9	8.15	6.05
40*	B	Ethyl	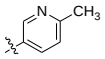	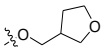	11	2	7.96	5.70
41	B	Ethyl	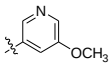	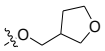	8	1.7	8.10	5.77
42*	B	Ethyl		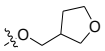	9	0.9	8.05	6.05
43	B	Ethyl		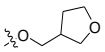	14	0.4	7.85	6.40
44	B	Ethyl		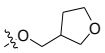	12	0.6	7.92	6.22
45	B	Ethyl	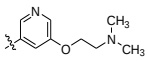	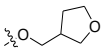	10	4	8.00	5.40
46	B	Ethyl	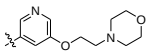	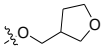	4	1	8.40	6.00
47	B	Ethyl		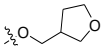	10	1.8	8.00	5.74
48	B	Ethyl		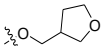	1	0.14	9.00	6.85
49	B	Ethyl		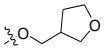	4.6	0.14	8.34	6.85
50	B	Ethyl	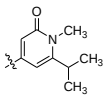	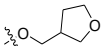	8	0.53	8.10	6.28
51	B	Ethyl	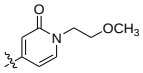	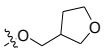	0.5	0.06	9.30	7.22
52*	B	Ethyl			47	5	7.33	5.30
53	B	Ethyl	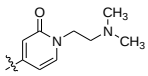	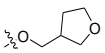	3	3.1	8.52	5.51
54	B	Ethyl	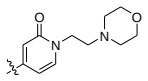	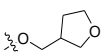	2.2	0.6	8.66	6.22
55	C	Allyl		H	160	16	6.80	4.80

* test set

Table 2. The statistical results of HQSAR models.

Activity	Descriptor	q^2	r^2	s	SEE	N	Hologram length
$\log(1/IC_{50})$	DA/C/A	0.62	0.91	0.36	0.17	6	353
log(1/MIC)	DA/B/C/A	0.60	0.90	0.41	0.20	6	71

A, atoms; B, bonds; C, connections; DA, donor and acceptor; q^2, leave-one-out (LOO) cross-validated correlation coefficient; r^2, non-cross-validated correlation coefficient; N, optimum number of components; s, standard error of prediction; SEE, standard error of estimate

Table 3. The statistical results of CoMFA and CoMSIA models.

Activity	Descriptor	q^2	r^2	S	SEE	F	N	Fraction
$\log(1/IC_{50})$	CoMFA S/E	0.47	0.90	0.42	0.18	96.69	4	40/60
	CoMSIA S/E/H/D	0.62	0.98	0.36	0.08	388.93	6	15/33/27/25
log(1/MIC)	CoMFA S/E	0.33	0.77	0.50	0.30	46.12	3	40/60
	CoMSIA S/E/H	0.39	0.73	0.48	0.32	58.40	2	17/38/45

S steric field; E electrostatic field; H hydrophobic field; D hydrogen donor field; A hydrogen acceptor field; q^2, leave-one-out (LOO) cross-validated correlation coefficient; r^2, non-cross-validated correlation coefficient; N optimum number of components; s standard error of prediction; SEE standard error of estimate; F F-test value

Table 4. Experimental and predicted activities for training and test set in CoMSIA and HQSAR models.

Cpd.	Scaffold	log(1/IC_{50})					log(1/MIC)		
		Exp.	CoMSIA	Res.	HQSAR	Res.	Exp.	HQSAR	Res.
1	A	7.96	8.01	-0.05	7.95	0.00	5.89	5.81	0.08
2*	A	7.70	7.92	-0.22	7.61	0.09	5.52	5.60	-0.08
3	A	7.80	7.86	-0.06	7.98	-0.18	6.10	6.19	-0.09
4	A	6.66	6.57	0.09	6.61	0.06	4.90	4.99	-0.08
5*	A	8.60	8.20	0.40	8.51	0.10	6.70	6.25	0.44
6	A	7.64	7.61	0.03	7.75	-0.11	5.70	5.52	0.18
7	A	8.00	8.05	-0.05	8.03	-0.03	4.96	4.77	0.19
8	A	7.64	7.64	0.00	7.75	-0.11	5.00	5.07	-0.07
9	A	8.22	8.28	-0.06	7.99	0.23	5.40	5.15	0.25
10	A	7.82	7.71	0.12	7.75	0.08	4.68	5.17	-0.49
11	A	8.40	8.43	-0.03	7.97	0.43	5.40	5.68	-0.29
12	A	7.70	7.66	0.03	7.54	0.16	5.80	5.84	-0.04
13	A	8.30	8.29	0.02	8.39	-0.09	6.30	6.25	0.05
14*	A	8.30	8.12	0.19	8.70	-0.40	6.52	6.41	0.12
15	A	8.60	8.60	0.00	8.63	-0.03	6.52	6.59	-0.07
16	A	7.08	7.08	-0.01	7.09	-0.02	5.05	5.10	-0.05
17	A	7.52	7.57	-0.04	7.52	0.00	5.70	5.36	0.34
18	A	7.40	7.40	-0.01	7.76	-0.36	5.70	5.31	0.39
19	A	7.40	7.45	-0.05	7.43	-0.03	5.52	5.46	0.06
20*	A	7.60	7.94	-0.34	7.55	0.05	5.10	5.24	-0.14
21	A	7.30	7.39	-0.08	7.32	-0.02	5.00	5.09	-0.09
22	A	7.40	7.39	0.01	7.49	-0.09	5.14	5.37	-0.24
23	A	7.85	7.85	0.01	7.70	0.16	5.52	5.50	0.02
24	B	7.66	7.65	0.01	7.75	-0.09	5.70	5.91	-0.21
25	B	8.43	8.41	0.03	8.67	-0.24	6.57	6.69	-0.12
26	B	7.06	7.09	-0.03	7.03	0.02	5.10	5.02	0.08
27	B	7.34	7.39	-0.05	7.41	-0.07	5.00	5.25	-0.25
28	B	7.60	7.62	-0.02	7.58	0.03	5.55	5.54	0.02
29	B	7.92	7.90	0.02	7.64	0.28	5.89	5.68	0.21
30	B	8.30	8.33	-0.03	7.98	0.32	5.89	6.07	-0.18
31	B	8.05	7.98	0.07	7.97	0.07	6.04	6.13	-0.09
32*	B	7.89	7.89	0.00	7.78	0.11	5.81	5.93	-0.12
33	B	7.41	7.23	0.17	7.72	-0.31	6.04	5.88	0.16
34	B	7.77	7.77	0.00	7.67	0.10	6.17	6.04	0.13
35	B	8.00	7.94	0.06	8.07	-0.07	6.70	6.57	0.12
36*	B	7.52	7.83	-0.31	7.29	0.23	5.70	5.68	0.02
37	B	7.52	7.57	-0.04	7.39	0.14	6.00	5.97	0.03
38	B	7.05	7.03	0.01	7.05	0.00	5.46	5.54	-0.09
39	B	8.15	8.22	-0.07	8.10	0.06	6.05	6.19	-0.14
40*	B	7.96	8.15	-0.19	7.97	-0.01	5.70	5.95	-0.25

41	B	8.10	8.19	-0.10	8.19	-0.09	5.77	5.72	0.05
42*	B	8.05	8.24	-0.19	7.99	0.05	6.05	6.02	0.03
43	B	7.85	7.93	-0.08	7.97	-0.11	6.40	5.98	0.41
44	B	7.92	7.91	0.01	8.18	-0.26	6.22	6.39	-0.17
45	B	8.00	7.91	0.09	8.14	-0.14	5.40	5.51	-0.12
46	B	8.40	8.41	-0.01	8.30	0.10	6.00	5.82	0.18
47	B	8.00	8.06	-0.06	8.11	-0.11	5.74	5.75	0.00
48	B	9.00	8.75	0.25	8.72	0.28	6.85	6.77	0.08
49	B	8.34	8.36	-0.02	8.41	-0.07	6.85	6.97	-0.12
50	B	8.10	8.24	-0.14	8.16	-0.06	6.28	6.39	-0.11
51	B	9.30	9.22	0.09	9.15	0.16	7.22	7.07	0.15
52*	B	7.33	7.67	-0.35	7.34	-0.01	5.30	5.72	-0.42
53	B	8.52	8.58	-0.05	8.58	-0.05	5.51	5.75	-0.24
54	B	8.66	8.65	0.01	8.58	0.08	6.22	5.97	0.25
55	C	6.80	6.80	-0.01	6.83	-0.04	4.80	4.90	-0.10

*test set

Table 4. Binding free energy of thiazole urea core derivatives from MM-GBSA and waterswap calculations.

Cpd.	IC_{50}(nM)	Energy (kcal/mol)				
		$\Delta G_{Exp.}$*	ΔH	$T\Delta S$	$\Delta G_{MM\text{-}GBSA}$	$\Delta G_{waterswap}$
25	3.7	-11.58	-49.25	-21.24	-28.01	-36.57
26	88	-9.69	-46.56	-25.58	-20.98	-32.12
30	5	-11.40	-49.50	-17.58	-31.92	-33.74
35	10	-10.99	-48.89	-20.73	-28.16	-34.62
51	0.5	-12.77	-59.24	-21.86	-37.38	-45.38
55	160	-9.33	-48.48	-18.69	-29.79	-23.81

*Experimental binding free energy ($\Delta G_{Exp.}$) was calculated from $\Delta G_{Exp.} = -RT\ln[IC_{50}]$. Whereas, R is universal gas constant (1.988 kcal/mol) and T is temperature in Kevin (300 K).

Table 5. Predicted biological activities, docking score and pharmacokinetic prediction of novel thiazole urea derivatives

	Compound 51	**D007**	**D063**
HQSAR-IC_{50}	8.93	8.40	8.01
HQSAR-MIC	6.63	6.21	6.51
Autodock 4.2 docking score (kcal/mol)	-8.62	-9.66	-7.97
BBB	0.02	0.05	0.04
Caco2	38.87	15.72	12.58
CYP2C19 inhibition	Non	Non	Non
CYP2C9 inhibition	Non	Inhibitor	Non
CYP2D6 inhibition	Non	Non	Non
CYP2D6 substrate	Non	Non	Non
CYP3A4 inhibition	Non	Non	Non
CYP3A4 substrate	Substrate	Weakly	Substrate
HIA	94.70	90.50	87.84
MDCK	4.64	0.89	17.99
Pgp inhibition	Non	Non	Non
PPB	49.66	56.20	75.19
Ames test	mutagen	mutagen	mutagen
Carcino Mouse	negative	negative	negative
Carcino Rat	negative	negative	positive
hERG inhibition	low risk	medium risk	low risk

BBB: Indicates BB (Cbrain/Cblood) ratio. Value > 0.1 suggested moderate absorption to CNS

Caco2 permeability: Value of the Pcaco2 (nm/sec) < 4 indicates low permeability.

HIA: Calculated HIA at pH 7.4: Value between 70–100% indicates fair absorption

PPB: Plasma protein binding: Value > 90% indicates strong protein binding

MDCK cell level <25, the molecule is having low permeability

Figure captions

Figure 1. General structural scaffolds of thiazole urea core derivatives.

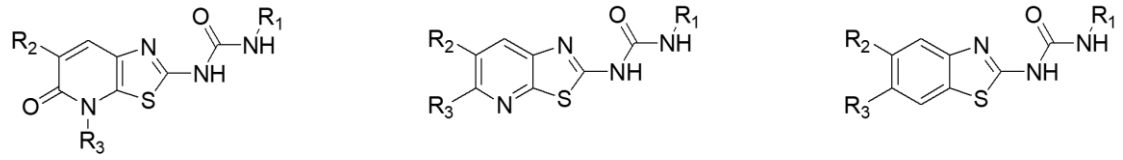

Thiazolopyridinone urea (Scaffold A)

Thiazolopyridine urea (Scaffold B)

Benzothiazole urea (Scaffold C)

Figure 2. Plot of experimental versus predicted biological values from each best IC_{50} CoMSIA (a), IC_{50} HQSAR (b) and MIC HQSAR model (c).

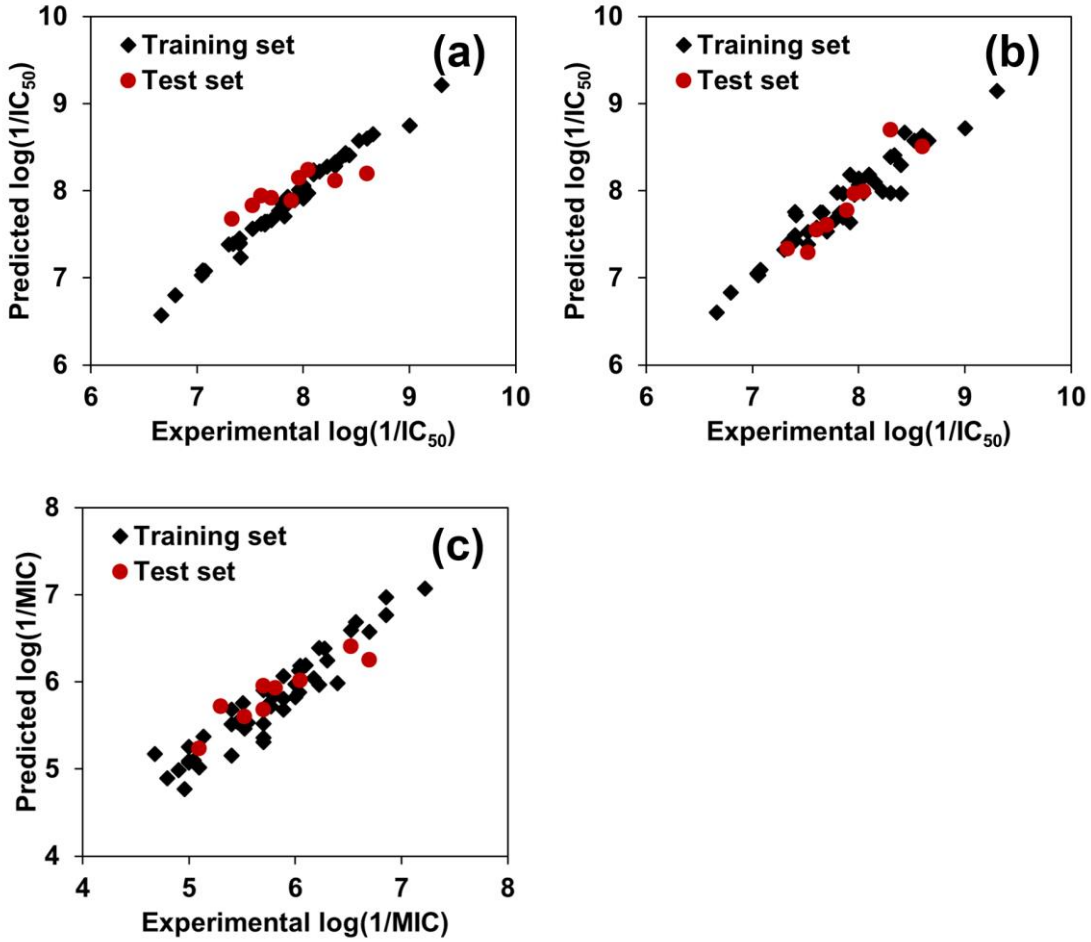

Figure 3. HQSAR contribution of thiazole urea core compounds derived from IC_{50} HQSAR model.

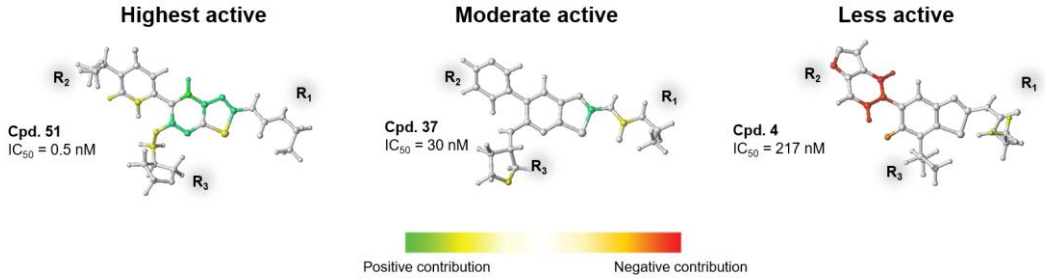

Figure 4. HQSAR contribution of thiazole urea core compounds derived from MIC HQSAR model.

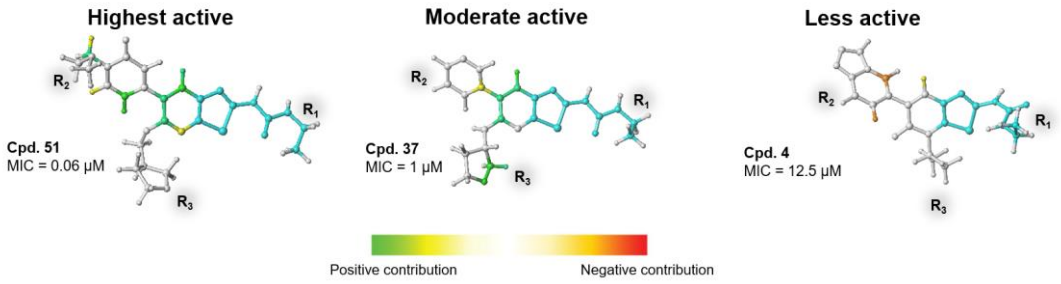

Figure 5. CoMSIA contour maps derived from the best IC_{50} CoMSIA model.

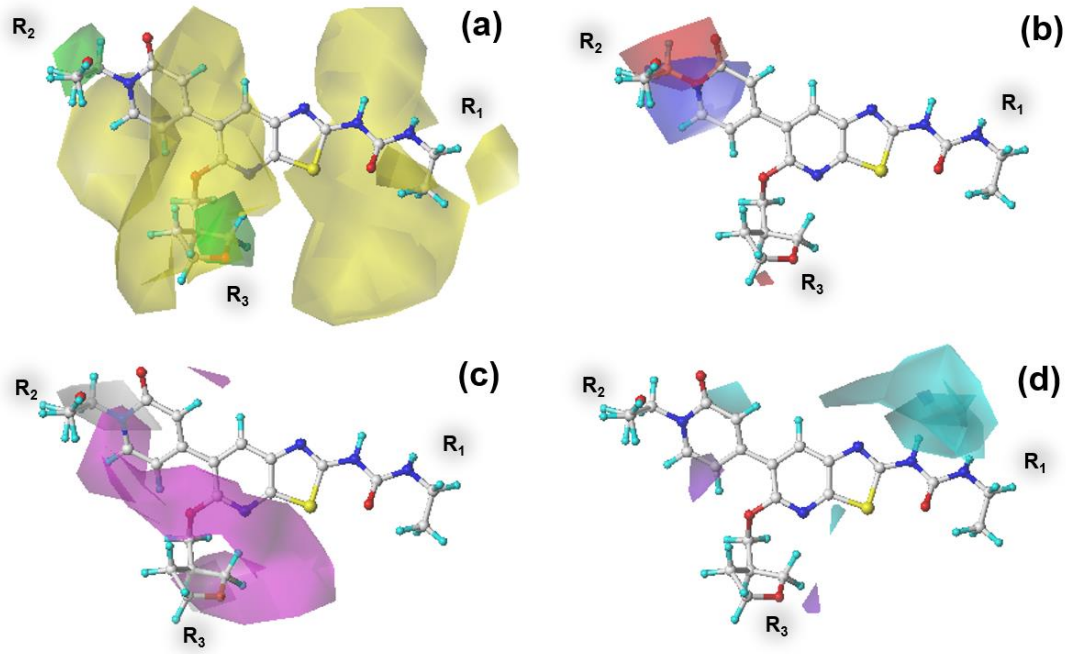

Figure 6. RMSD plotted of GyrB ATPase complexed with thiazole urea core derivatives; compound **25** (a), compound **26** (b), compound **30** (c), compound **35** (d), compound **51** (e) and compound **55** (f).

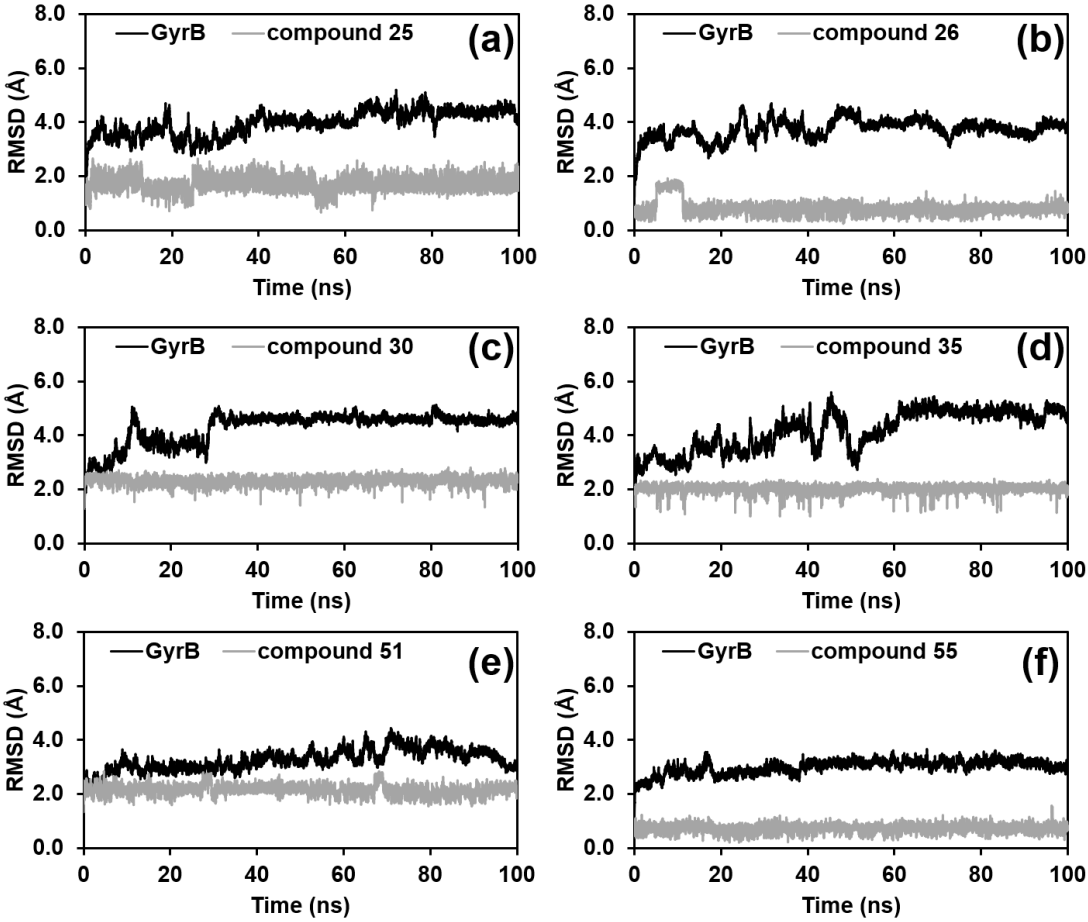

Figure 7. Correlation between experimental binding free energy and calculated binding free energy obtained from MM-GBSA (a) and waterswap calculation (b).

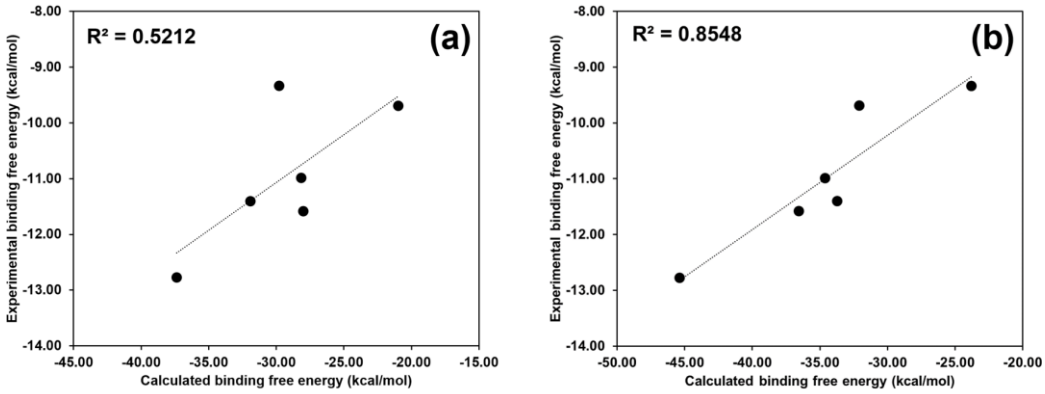

Figure 8. The binding mode and binding interactions of the highest active compound **51** obtained from MD simulations. Red and yellow dot line indicated hydrogen bond and cation-pi interactions, respectively.

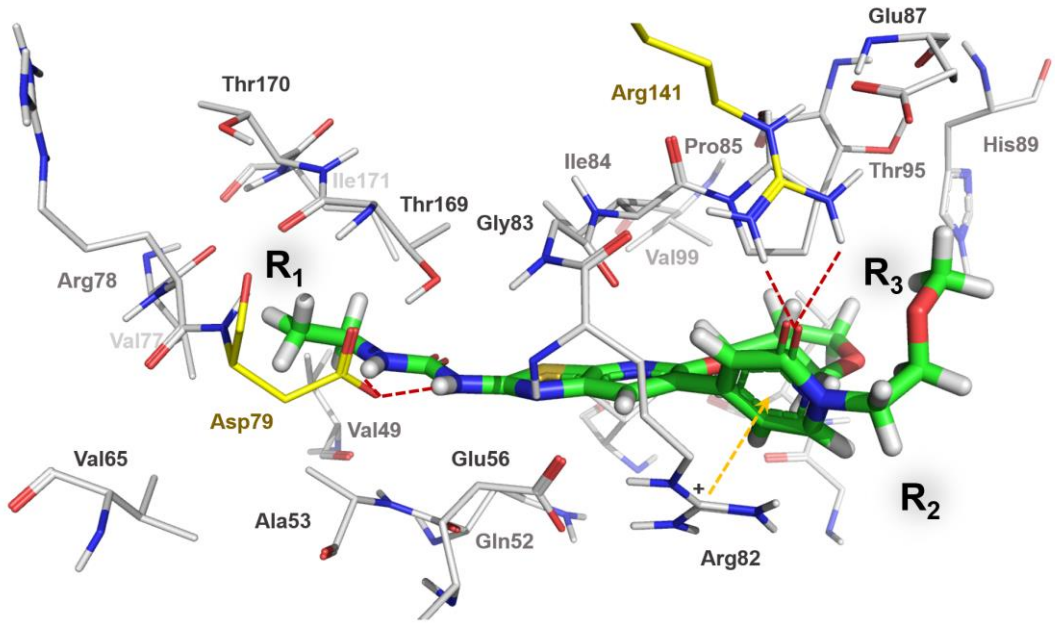

Figure 9. The binding interaction energy profile of thiazole urea core derivatives obtained from MM-GBSA calculations.

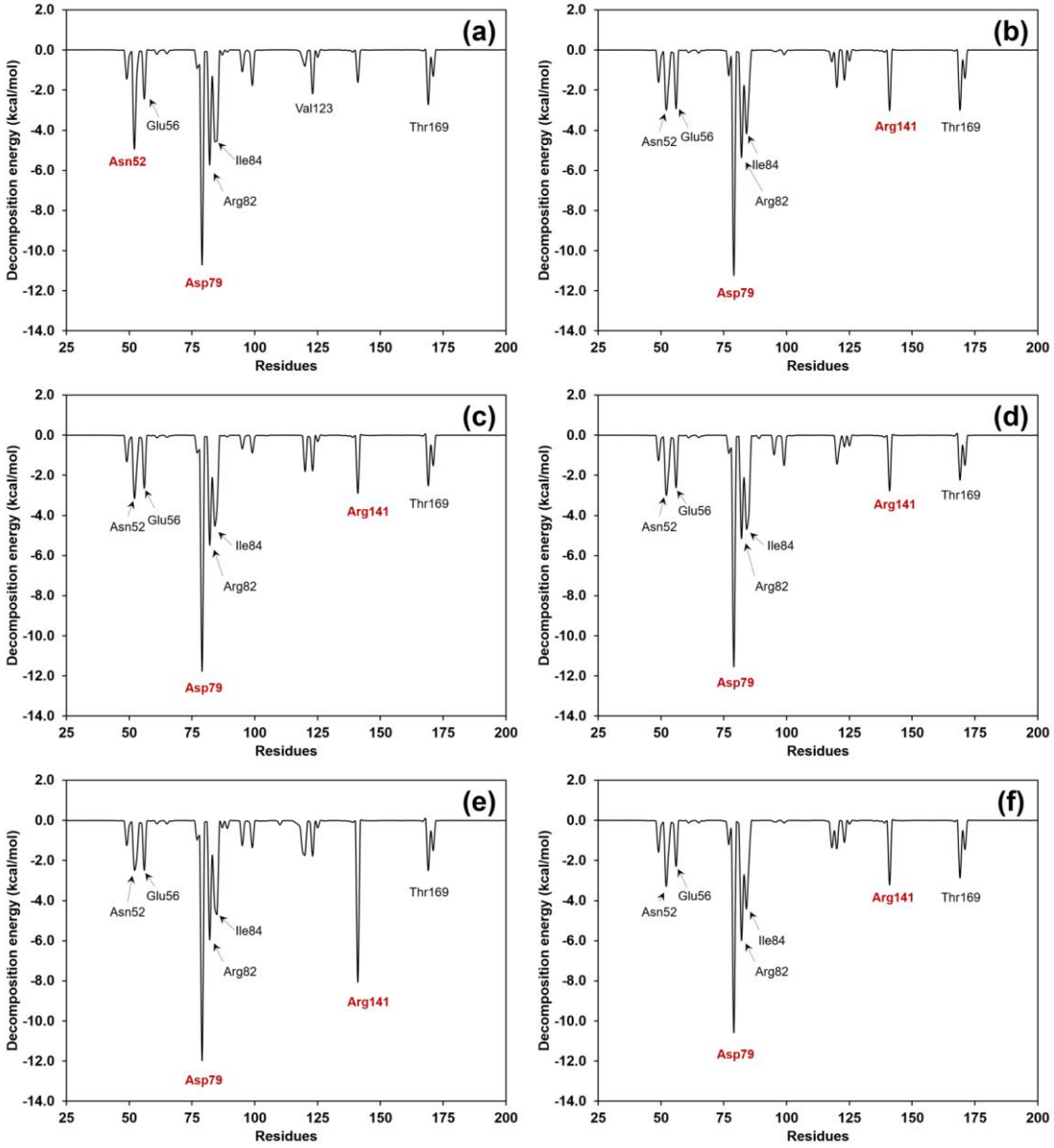

Figure 10. The hydrogen bond contribution obtained from MD simulations of thiazole urea core derivatives in GyrB ATPase domain.

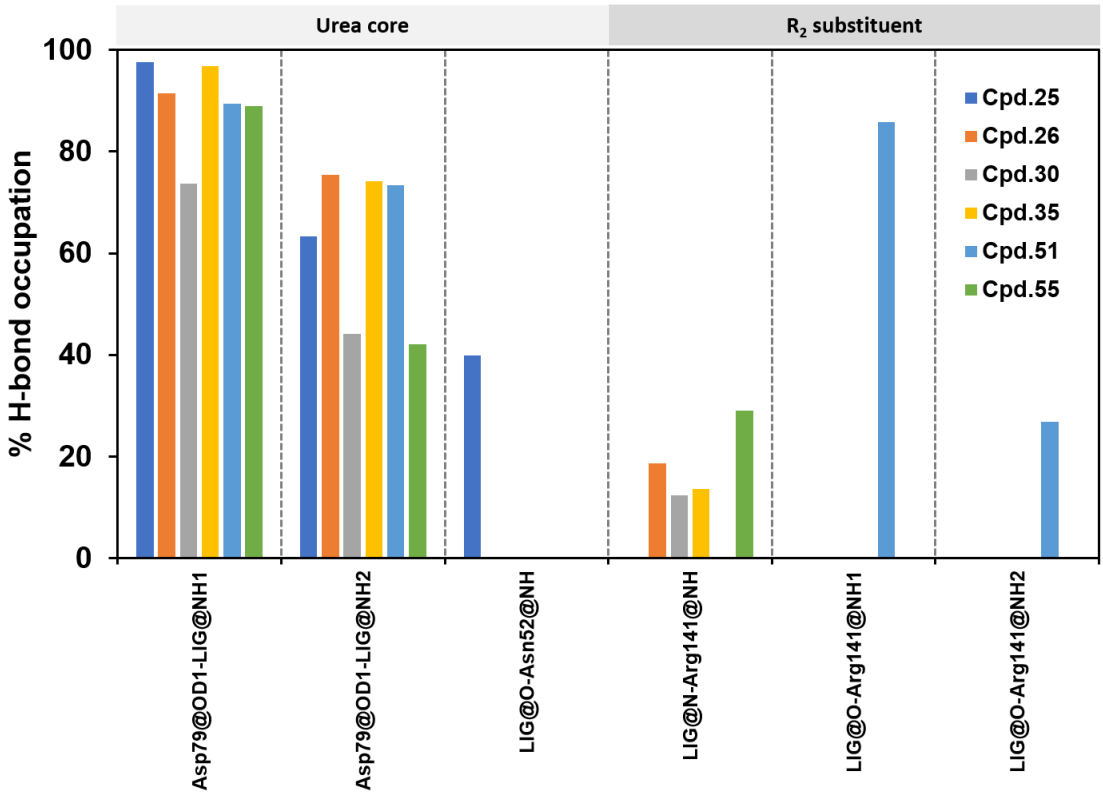

Figure 11. The key structural feature of thiazole urea cores for good IC_{50} and MIC correlation summarized from HQSAR, CoMSIA and MD simulations results. Red and black letters indicate the results obtained from QSAR (HQSAR and CoMSIA) and MD simulations results, respectively.

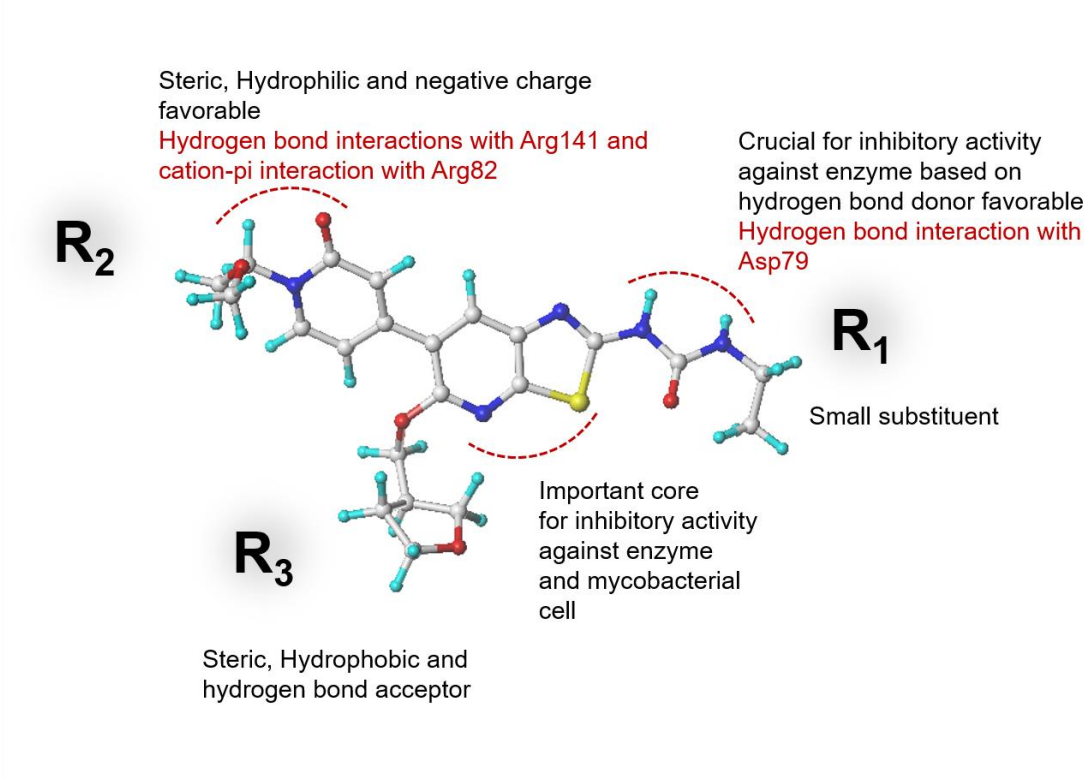

Figure 12. Structure and drug-like properties of novel thiazole urea derivatives.

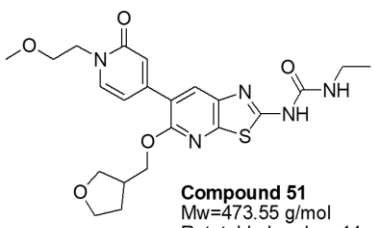

Compound 51
Mw=473.55 g/mol
Rotatable bonds = 11
H-bond acceptors = 7
H-bond donors = 2
XlogP3 = 1.39

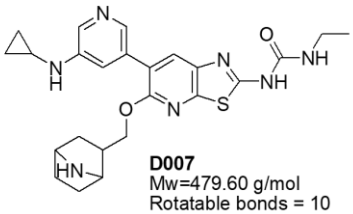

D007
Mw=479.60 g/mol
Rotatable bonds = 10
H-bond acceptors = 6
H-bond donors = 4
XlogP3 = 3.33

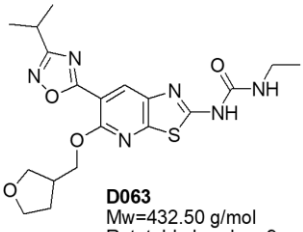

D063
Mw=432.50 g/mol
Rotatable bonds = 9
H-bond acceptors = 8
H-bond donors = 2
XlogP3 = 2.93

Figure 13. The binding mode and binding interactions of the **D007** (a) and **D063** (b) obtained from molecular docking calculations. Red and yellow dot line indicated hydrogen bond and cation-pi interactions, respectively.